Discover Nano

RESEARCH Open Access

Biogenic α-Fe_2O_3 nanoparticles from *Sorghum bicolor* leaf extracts and assessment of the anticancer and antioxidant properties

Lerato D. Msimango[1,2], Mercy C. Ogwuegbu[2,3], Doctor M. N. Mthiyane[1,2] and Damian C. Onwudiwe[4,5*]

*Correspondence:
Damian C. Onwudiwe
Damian.Onwudiwe@nwu.ac.za
[1]Department of Animal Science, Faculty of Natural and Agricultural Science, North-West University, Mmabatho 2035, South Africa
[2]Food Security and Safety Focus Area, Faculty of Natural and Agricultural Sciences, North-West University, Mmabatho 2735, South Africa
[3]Department of Animal Science, Faculty of Agriculture, University of Nigeria, Nsukka 410001Enugu State, Nigeria
[4]Materials Science Innovation and Modelling (MaSIM), Faculty of Natural and Agricultural Sciences, North-West University, Mmabatho, South Africa
[5]Department of Chemistry, School of Physical and Chemical Sciences, Faculty of Natural and Agricultural Science, North-West University (Mafikeng Campus), Private Bag X2046, Mmabatho, South Africa

Abstract

The synthesis of nanomaterials has recently shifted toward environmentally benign approaches that mitigate the drawbacks of conventional chemical methods. In this context, plant-mediated green synthesis offers a sustainable and versatile alternative for producing nanoparticles with unique physicochemical properties and diverse applications. This study presents the green synthesis of hematite iron oxide nanoparticles (α-Fe_2O_3 NPs) using aqueous leaf extracts of *Sorghum bicolor*. The resulting nanoparticles were characterized using X-ray diffraction (XRD), UV–visible spectroscopy, scanning electron microscopy (SEM), transmission electron microscopy (TEM), and energy-dispersive X-ray spectroscopy (EDX). XRD analysis confirmed the formation of a crystalline rhombohedral hematite phase with an average crystallite size of 46.8 nm. SEM and TEM images revealed predominantly spherical particles with evident agglomeration, while EDX analysis confirmed iron (Fe) and oxygen (O) as the primary elemental constituents. Antioxidant activity assessed via the 2,2-diphenyl-1-picrylhydrazyl (DPPH) assay showed a concentration-dependent radical scavenging effect, with higher α-Fe_2O_3 NP concentrations required to achieve 50% inhibition. Cytotoxicity studies on HeLa (cancer) and HEK293 (normal) cell lines indicated selective toxicity, with the nanoparticles preferentially affecting cancer cells while sparing healthy ones. Although the α-Fe_2O_3 NPs exhibited lower potency compared to the standard chemotherapeutic agent 5-fluorouracil, their concentration-dependent reduction in cell viability supports the hypothesis that cancer cells are particularly vulnerable to disruptions in iron homeostasis. This cost-effective and eco-friendly synthesis method underscores the potential of *Sorghum bicolor*-mediated α-Fe_2O_3 nanoparticles for future biomedical applications.

Keywords Green chemistry, Iron oxide, Biosynthesis, Cytotoxicity, Antioxidants

1 Introduction

Metal oxide nanoparticles obtained through green synthesis are gaining greater acceptability over those obtained through traditional chemical synthesis. The use of plant extracts for the green synthesis of metal oxide nanoparticles offers several environmental benefits compared to traditional methods, including the use of non-toxic reagents,

© The Author(s) 2025, corrected publication 2025. **Open Access** This article is licensed under a Creative Commons Attribution 4.0 International License, which permits use, sharing, adaptation, distribution and reproduction in any medium or format, as long as you give appropriate credit to the original author(s) and the source, provide a link to the Creative Commons licence, and indicate if changes were made. The images or other third party material in this article are included in the article's Creative Commons licence, unless indicated otherwise in a credit line to the material. If material is not included in the article's Creative Commons licence and your intended use is not permitted by statutory regulation or exceeds the permitted use, you will need to obtain permission directly from the copyright holder. To view a copy of this licence, visit http://creativecommons.org/licenses/by/4.0/.

environmental friendliness, reduced energy consumption, and ease of synthesis [1, 2]. The phytochemicals present in plant extracts act as natural reducing and capping agents, facilitating nanoparticle formation under ambient or mild reaction conditions, which in turn reduces energy consumption compared to high-temperature or high-pressure conventional methods [3]. This approach promotes the use of renewable and biodegradable resources, aligning with the principles of green chemistry and circular economy [4]. It supports waste valorization, especially when agro-waste or non-edible plant parts are used, further enhancing the environmental sustainability of the process. This is mainly because of their phytochemicals, such as flavonoids, terpenoids, carotenoids, and polyphenols present in plant parts– peels, stems, leaves, and fruits that serve as reducing agents during the synthesis [5, 6]. The biocompatibility of nanoparticles obtained through this technique makes them important materials in biological applications such as drug delivery, disinfection, anticancer agents, and antioxidant [7, 8].

Furthermore, this eco-friendly approach aligns with the principles of green chemistry and enhances sustainability by utilizing renewable, biodegradable resources. Consequently, it contributes to cleaner production processes and supports the development of sustainable nanomaterials with lower environmental footprints [9, 10].

Although metal oxide nanoparticles could potentially induce oxidative stress, some nanoparticles exhibit excellent activity as anticancer and antioxidants, such as CeO_2, ZnO, NiO, Co_3O_4, and ZnO–MgO–CaO [11–14]. As antioxidants, metal oxides mimic the activity of natural antioxidant enzymes by directly scavenging reactive oxygen species (ROS) such as superoxide radicals and hydrogen peroxide, making them suitable agents for therapeutic application against oxidative stress-related diseases [15, 16]. Interestingly, metal oxides can act as effective anticancer agents primarily by generating reactive oxygen species (ROS), inducing oxidative stress, triggering apoptosis, and interfering with cellular processes through the release of metal ions. Separately, they can also exhibit antibacterial properties by disrupting bacterial cell membranes and generating ROS. This makes them potential alternatives to traditional antibiotics in overcoming antimicrobial resistance [16, 17].

Among the several green-synthesized metal oxides that have been explored for biomedical applications [12–14], iron oxides have gained much interest because of their high biocompatibility, and unique physical characteristics such as low susceptibility to oxidation, long blood half-life, and flexible surface chemistry [18, 19]. Superparamagnetic iron oxide nanoparticles incorporated with mesoporous silica nanoparticles, with the surface functionalized by NH_2-bonding have been used as oxaliplatin loading and colon cancer treatment [20]. Sabouri et al. [21] reported amino-functionalized core-shell magnetic iron oxide nanoparticles used for inhibiting cancer cells. They have also been used as potential nanocarriers in drug delivery systems [22].

The hematite phase (α-Fe_2O_3) has particularly gained much traction compared to other oxides because of its exceptional stability under ambient conditions, making it highly resistant to corrosion and degradation. It is also relatively cheap and abundantly available in nature, making it an ideal material for several applications [23–25]. The green synthesis of α-Fe_2O_3, therefore, provides a facile and less-toxic route to obtaining a potentially effective antioxidant and anticancer agent.

Herein, in this study we have explored the use of aqueous extracts of *Sorghum bicolor* as an anticancer and antioxidant agent. *Sorghum bicolor* is a flowering plant belonging

to the Poaceae family. It possesses biomolecules with therapeutic, functional, and nutraceutical properties that have been explored in the treatment of different ailments [26, 27]. The presence of these functional biomolecules makes extracts from *Sorghum bicolor* suitable for the synthesis of nanoparticles [3, 28, 29]. *Sorghum bicolor* leaf extract was chosen for the synthesis of α-Fe_2O_3 nanoparticles due to its rich phytochemical composition, which includes polyphenols, flavonoids, and alkaloids. These biomolecules facilitate the reduction of ferric ions and act as natural mediating agents, promoting the formation of stable nanoparticles. Additionally, *Sorghum bicolor* is an easily accessible, renewable, and eco-friendly resource, aligning with the principles of green chemistry and sustainable nanomaterial synthesis. Previous reports have also demonstrated the plant's efficacy in the biosynthesis of metal-based nanoparticles, further supporting its selection for this study. The potential anticancer and antioxidant activities of this nanomaterial could lead to the production of materials that could serve as alternatives to traditional drugs.

2 Materials and methods

2.1 Plant collection and reagents

Sorghum bicolor leaf was harvested from the North-West University research farm at Mafikeng Campus. High purity (99%) ferrous sulfate heptahydrate ($FeSO_4{\cdot}7H_2O$) and sodium hydroxide (NaOH) were purchased from Merck, RSA, and used as received.

2.2 Preparation of aqueous plant extract

The fresh *Sorghum bicolor* leaves were harvested, chopped into smaller pieces, and dried at room temperature for 28 days. The dried leaves were pulverised using a dry blender, and thereafter about 8 g of the powder was mixed with 100 mL of distilled water, followed with heating at 85 °C for 1 h while vigorously stirring. The mixture was allowed to cool to room temperature, filtered using no. 1 Whatman filter paper, and kept for further use [30]. Figure 1 presents the schematic steps for the extraction and synthesis processes.

2.3 Qualitative phytochemical screening of *Sorghum bicolor leaves*

The presence of various phytochemical constituents in *Sorghum bicolor* leaves was assessed using procedures as outlined in previous reports in the literature [31, 32].

2.3.1 Saponin test

Approximately 0.3 g of the leaf powder was mixed with 30 mL of distilled water, heated in a water bath for 10 min, and then filtered through Whatman No. 42 filter paper (125 mm). To ensure the stability of the resulting foam, about 10 mL of the filtrate was mixed with 5 mL of distilled water and vigorously shaken. Three drops of olive oil were then added to the resulting froth, and the mixture was stirred vigorously to observe the formation of a stable emulsion, indicating the presence of saponins.

2.3.2 Terpenoid test

About 0.3 g portion of the leaf powder was soaked in 30 mL of distilled water and left to stand for 2 h. Subsequently, 5 mL of the extract was mixed with 2 mL of chloroform and

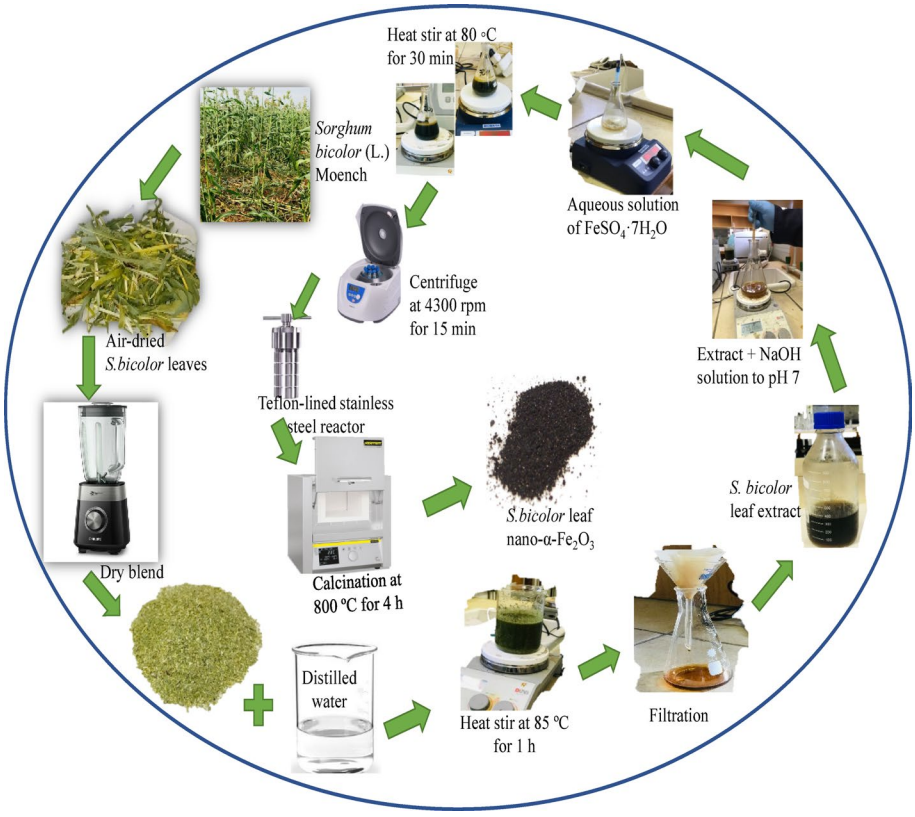


Fig. 1 The schematic representation of the preparation of aqueous extract of *Sorghum bicolor* leaf and the green synthesis of α-Fe_2O_3 -NPs

3 mL of conc. sulphuric acid to form a separate layer. The appearance of a reddish-brown coloration at the interface was indicative of terpenoids.

2.3.3 Flavonoid test

About 0.3 g portion of the leaf powder was soaked in 30 mL of distilled water, heated in a water bath for 2 h, and filtered using Whatman No. 42 filter paper (125 mm). To 10 mL of this aqueous filtrate, 5 mL of 1 M ammonia solution was added, followed by 5 mL of conc. sulphuric acid. A transient yellow coloration signified the presence of flavonoids.

2.3.4 Tannins test

A 0.3 g portion of *Sorghum bicolor* leaf powder was weighed and heated in 30 mL of distilled water using a water bath for 10 min. The mixture was then filtered, and to 5 mL of the resulting filtrate, three drops of 0.1% ferric chloride solution were added. The resulting colour was observed for a brownish-green or blue-black hue, indicating the presence of tannins.

2.4 Synthesis of hematite α-Fe_2O_3 nanoparticles

α-Fe_2O_3 nanoparticles were prepared by following a previously reported procedure with slight modification [33]. In brief, 3.0 g of $FeSO_4 \cdot 7H_2O$ was dissolved in 100 mL distilled water and was heated to 80 °C. While vigorously stirring the solution, 30 mL of the fresh aqueous extract of *Sorghum bicolor* leaf, whose pH has been adjusted to 10 using NaOH solution, was added dropwise. The resultant mixture was stirred for 30 min, and a

caramel colour was observed. The final volume of the reaction solution was set to 70 mL and transferred to a Teflon-lined stainless-steel reactor (Autoclave) and heated to 145 °C for 2 h. The obtained particles were centrifuged at 4300 rpm for 20 min, rinsed twice with distilled water, and then followed with ethanol. The precipitate was transferred to a clean crucible and calcinated at 800 °C for 4 h, giving about 65% yield. The synthesized nanoparticles were kept for characterization.

2.5 Characterization of α-Fe_2O_3-NPs

The X-ray diffraction (XRD) technique was used to analyse the crystalline structure of the nanoparticles (NPs), using a Bruker D8 Advanced diffractometer. Measurements were performed at room temperature over a 2θ diffraction angle range of 20° to 70°, with a step size of 0.05° and a counting time of 5 s per step, utilizing a Cu radiation source and Bragg-Brentano geometry. The UV-visible spectral analysis of α-Fe_2O_3 NPs was conducted in ethanol (as solvent) using a PROVE 300 with a resolution of 1 nm, across the wavelength range of 200 to 800 nm. Functional groups involved in the reduction process by the leaf extract were identified using a Cary 630 (Agilent, Palo Alto, USA) Fourier Transform Infrared (FTIR) spectroscopy, which was measured in the spectral range of 500–4000 cm^{-1}. The powdered leaf samples were used as the input material.

The external morphology of the nanoparticles was examined using scanning electron microscopy (SEM) (JSM 6510LV JEOL). Transmission electron microscopy (TEM) was utilized to determine the size and morphology of the NPs, using a JEOL-2100 TEM (100/120 kV) operating at 200 kV. For sample preparation, the NPs were dispersed in isopropanol and subjected to 10–15 min of sonication. Thereafter, a drop of the dispersion was placed onto a carbon grid, and the samples were analyzed after the solvent had evaporated. ImageJ software was used to determine the average particle size in the solid state.

2.6 Cytotoxicity evaluation

The cytotoxic effects of α-Fe_2O_3-NPs were assessed based on the method described in [34], with some modifications. HeLa and HEK293 cell lines used for the assay were sourced from ATCC, Manassas, USA. Liver and kidney cell lines were grown in 25 cm^2 tissue culture flasks with a medium containing 10% foetal bovine serum, 100 µg/mL streptomycin, and 100 U/mL penicillin. For the MTT assay, 2.5×10^2 cells/well in 100 µL of DMEM were plated in a 96-well plate and incubated overnight at 37 °C. The nanoparticles were added at concentrations of 10, 25, 50, and 100 µg/mL, and the cells were incubated for 48 h at 37 °C. 5-fluorouracil (5-FU) served as the reference treatment. After 48 h, the medium was replaced with fresh media containing 10% MTT reagent, and the cells were incubated for an additional 4 h at 37 °C. Following incubation, the formazan crystals formed were dissolved in 100 µL of dimethyl sulfoxide (DMSO), and the absorbance was measured at 570 nm, with DMSO as the blank. The experiment was conducted in triplicate, and the average absorbance was calculated. Cell viability was determined using the Eq. (1).

$$\% \text{ Cell viability} = \text{Treated cells/Untreated cells} \times 100 \quad (1)$$

2.7 Antioxidant activity evaluation

The radical scavenging activity of the α-Fe_2O_3 -NPs was assessed using a modified version of the DPPH assay, based on the procedure outlined in [8], with some adjustments. To prepare the DPPH solution, about 12.8 mg of DPPH was dissolved in methanol (50 mL) to reach a conc. of 0.032 mM, and the solution was allowed to incubate in the dark for 30 min. Thereafter, α-Fe_2O_3 solutions at various concentrations (31.25, 62.5, 125, 250, 500, and 1000 ppm) were prepared in 1 mL of methanol. Then, 1 mL of the DPPH solution was introduced into each α-Fe_2O_3 solution, while the blank consisted of only the DPPH solution and methanol. Absorbance was recorded at 540 nm, with the control being the 0.032 mM DPPH solution. The experiment was performed in triplicate, and the percentage inhibition was determined using Eq. 2.

$$\%\text{Inhibition} = (A_c - A_s)/A_c \times 100\% \quad (2)$$

where (A_c) is the absorbance of the control, and (A_s) represents the sample's absorbance.

3 Results and discussion

3.1 Synthesis mechanism

The phytochemical analysis of the leaf extract of *Sorghum bicolor* revealed the presence of bioactive compounds, including flavonoids, alkaloids, tannins, saponins, and triterpenes, as shown in Table 1, and similar to previous reports [35, 36]. These phytochemicals have the capacity to reduce metal ions in a metallic salt solution to their zero valent state. A plausible mechanism for the formation of the α-Fe_2O_3 NPs is presented in Fig. 2. In the first step of the process, the Fe^{2+} was reduced to Fe^0 while the oxidized product of the polyphenolic compound was formed. The polyphenols present in plant extracts have been reported to have a high value of standard reduction potential (between 0.534 and 0.540 V) [37] that is enough to reduce metals such as iron (standard potential −0.44 V [38]) to their respective nanoparticles [38, 39]. In the second step, due to the high instability of the Fe^0, an immediate oxidation to Fe^{3+} occurred. This is a typical metal core-shell oxidation reaction, and similar processes have been reported [40]. Due to the presence of NaOH and adjustment of the pH to the basic medium, the formation of $Fe(OH)_3$ occurred, subsequently forming Fe(OOH). The calcination process removed a water molecule and resulted to the hematite nanoparticles as presented in Eq. 3.

$$2Fe(OOH) \longrightarrow \alpha\text{-}Fe_2O_3 + H_2O \quad (3)$$

3.2 Fourier transform infrared (FTIR) analysis

The FTIR spectrum of *Sorghum bicolor* leaf represented in Fig. 3a shows broad and sharp peaks around 3271 and 1630 cm^{-1}, which are associated with the O-H stretching and

Table 1 Qualitative analysis of phytochemicals present in *Sorghum bicolor* leaves

Compounds	*M. azedarach* seed
Saponin	+
Terpenoids	++
Flavonoids	++
Tannins	++

Heavily present……++
Present……+
Absent……–

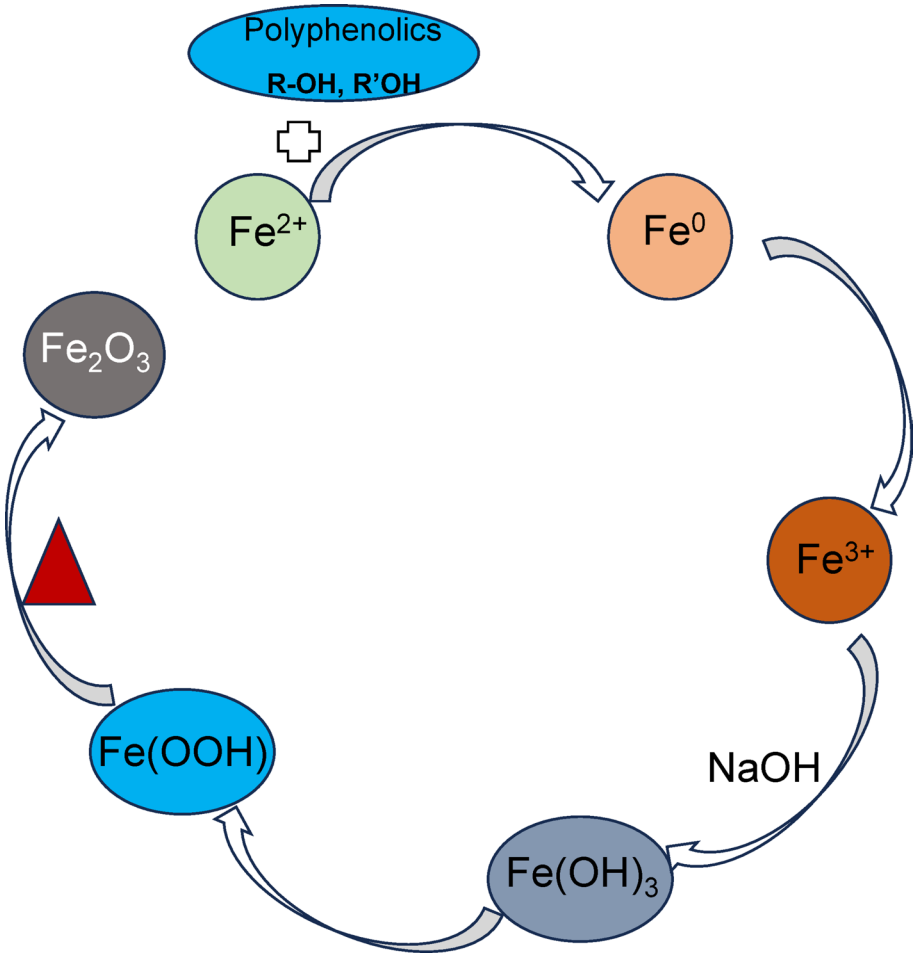


Fig. 2 A plausible mechanism for formation of the α-Fe_2O_3 NPs using aqueous extract of *Sorghum bicolor* leaves

bending vibrations, respectively. These peaks are associated with the water molecules from the raw cellulose [41–43]. Symmetric and asymmetric C–H stretching vibrations of unsaturated SP^2 hybridised hydrocarbon were identified around 2917 and 2851 cm-^{1}, respectively [44]. The band around 1735 cm-^{1} may be ascribed to the presence of carbonyl C = O stretch of hemicellulose [45–48], while the band at 1027 cm-1 reveals the C-O stretch vibrations [49]. These peaks are indicative of the *Sorghum* fibre's hydrophilic properties. The FTIR spectrum of the biosynthesized α-Fe_2O_3 NPs is presented in Fig. 3b. The peaks at 527 and 435 cm^{-1} could be ascribed to the Fe–O stretching and Fe–O bending vibrations in the crystalline lattice of α-Fe_2O_3 [50, 51]. Bands between 400 and 600 cm^{-1} are often ascribed to the stretching vibration mode that is associated with the metal-oxygen. The peak around 2335 cm^{-1} is related to the asymmetric stretching vibration of the O–C–O group, likely due to the presence of absorbed CO_2 on the nanoparticles [52]. This may be confirmed by the appearance of the band around 1102 cm^{-1} [53]. The absence of the bands observed around 3271 and 1630 cm^{-1}, which are attributed to the O–H vibrations from the plant extract, as well as the C–H vibrational bands are indicative of the disappearance of the phytochemical components of the materials at the high calcination temperature.

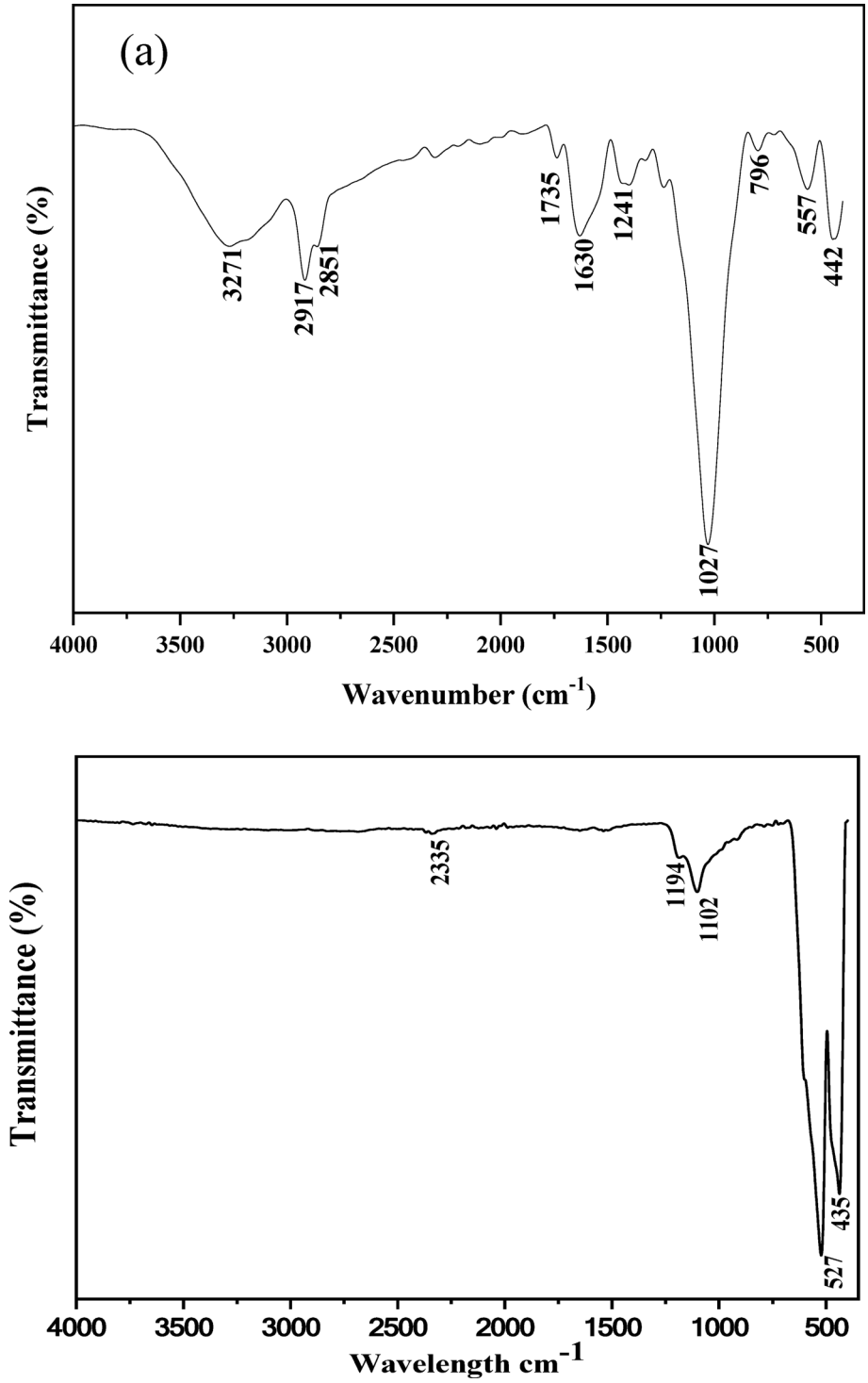


Fig. 3 FTIR spectra of **a** extract of *Sorghum bicolor* leaves and **b** α-Fe_2O_3 NPs

3.3 X-ray diffraction analysis (XRD)

The XRD pattern of *Sorghum bicolor* leaf extract-mediated iron oxide nanoparticles is shown in Fig. 4. It shows diffraction peaks at 2θ values of (24.26°), (33.37°), (35.74°), (41.02°), (49.61°), (54.27°), (57.68°), (62.65°), and (64.20°), corresponding to the ((012), (104), (110), (113), (024), (116), (018), (214), and (300) planes of the rhombohedral

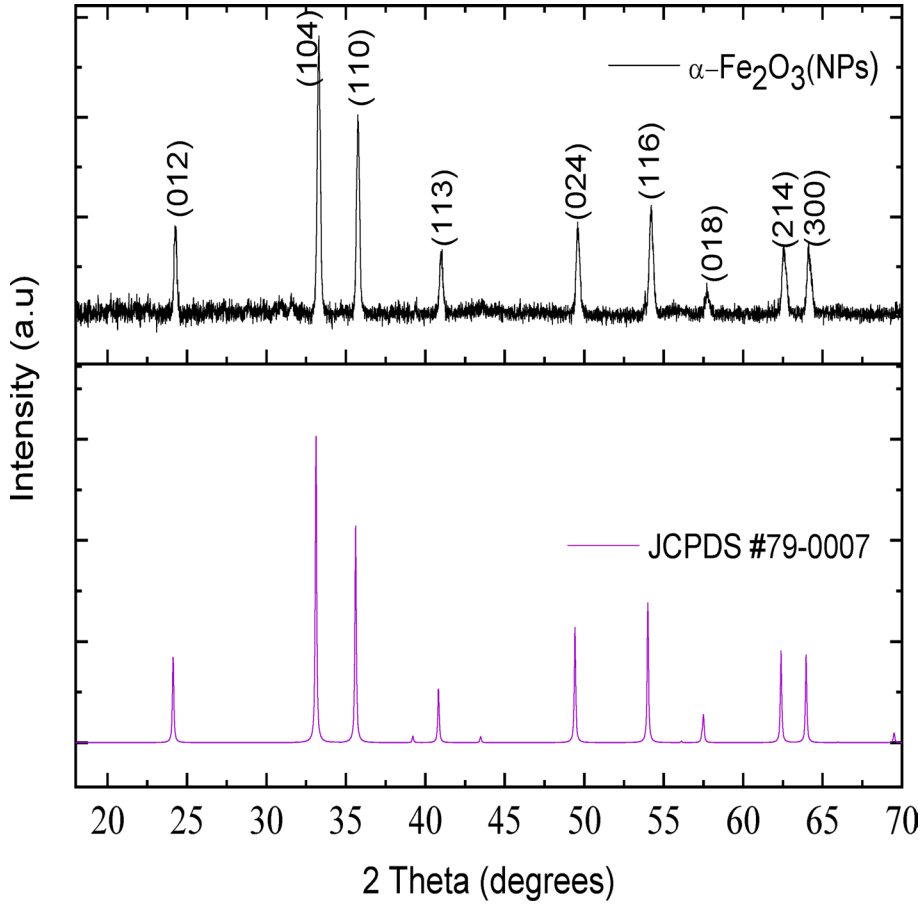


Fig. 4 XRD pattern of α-Fe_2O_3 NPs mediated by aqueous extract of *Sorghum bicolor* leaves

Table 2 Structural parameters of α-Fe_2O_3 obtained from Rietveld refinement

Sample	Grainsize (μm)	% Crystallinity	% Porosity	Surface area (m^2/g)
α-Fe_2O_3	2.791	89.94	0.134	0.0126

hematite phase of nanoparticles (α-Fe_2O_3) (JCPDS 79-0007) [54]. The absence of additional peaks in the XRD pattern confirms the high purity of the green-synthesized α-Fe_2O_3 nanoparticles. Furthermore, the intensity and sharpness of the peaks indicated that the nanoparticles were crystalline [55]. Using the Debye-Scherrer formula in Eq. 4, the crystallite size of the nanoparticles was estimated from the most predominant (104) plane of the synthesized hematite nanoparticles to be approximately 46.8 nm.

$$D = \frac{K\lambda}{\beta Cos\ \theta} \tag{4}$$

where, λ is the wavelength of the X-ray (1.5406 Å), K represents the shape factor (0.9), θ represents the diffraction angle given in degrees, and β is the full width at half maxima (FWHM) of the peaks of interest [56].

Rietveld refinement of the XRD data was performed using X'Per Highscore plus software to extract the structural details (Table 2). The α-Fe_2O_3 nanoparticles showed large grain size and good crystallinity, but low porosity. The large grain size could be due to

grain growth mechanisms, which often take place at high temperatures via diffusion and coalescence [57]. This is also responsible for the low porosity of the sample. A previous study showed that increasing hematite's calcination temperature results in a consistent increase in the crystal density of the phase. This was an indication of a decrease in the degree of disorder in the crystal lattice and growth of the binding energy of lattice oxygen [58].

3.4 UV-Vis spectra analysis

Figure 5a and b present the UV-visible absorption spectrum and the corresponding Tauc plots of the as-synthesized α-Fe_2O_3 NPs, respectively. As illustrated in Fig. 5a, the NPs exhibit an absorption peak around 265 nm and a weak absorption around 435 nm that broadens to 600 nm within the visible light region. A similar absorption band has been observed for α-Fe_2O_3 nanoparticles synthesized using various plant extracts, including the root extract of *Spondias dulcis* [59], and *Phoenix dactylifera* leaf extract [60]. The band gap energy of the α-Fe_2O_3 nanoparticles was determined using a Tauc plot (inset of Fig. 5b) and was obtained as 2.8 eV. This aligns closely with the previously reported value of 2.75 eV for α-Fe_2O_3 synthesized using henna extract [61], and 2.80 eV reported by Anit et al. [62]. The band gap energy of α-Fe_2O_3 can vary depending on factors such as synthesis method or introduction of foreign materials such as dopants.

3.5 Morphological studies

The morphological properties of the α-Fe_2O_3 nanoparticles were determined using both SEM and TEM characterization techniques. The SEM analysis showed that the NPs exhibited a distinctly spherical shape (Fig. 6a), while the higher magnification image (Fig. 6b) confirmed well-aggregated particles that are clustered together to form a uniform structure. This aggregation may be due to the interaction of the charges present on the surface of the nanoparticles, which has been reported to increase as the size of the particles within the nanometric regime [63]. The high-temperature calcination reaction of the nanoparticles has also been reported to increase the surface reactivity, thereby enhancing aggregation [64]. Kaur et al. [65] reported the green synthesis of nanoparticles using the extract of *Carica papaya*, and attributed the aggregation of NPs to the

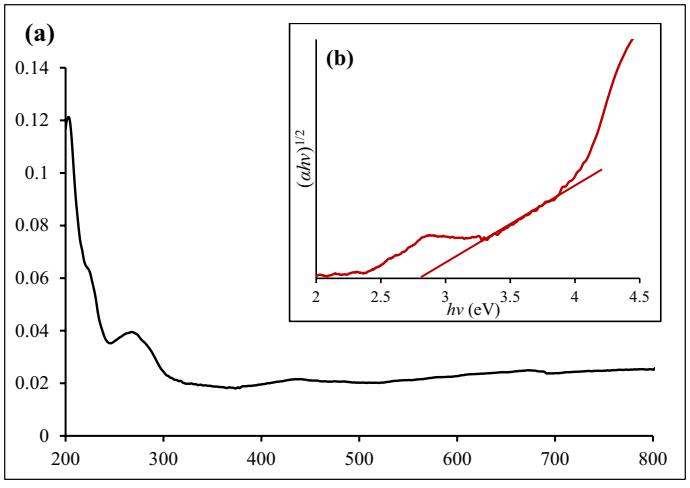


Fig. 5 **a** The UV-visible spectrum and **b** Tauc plots of the α-Fe_2O_3 NPs prepared from the aqueous extract of *Sorghum bicolor* leaves

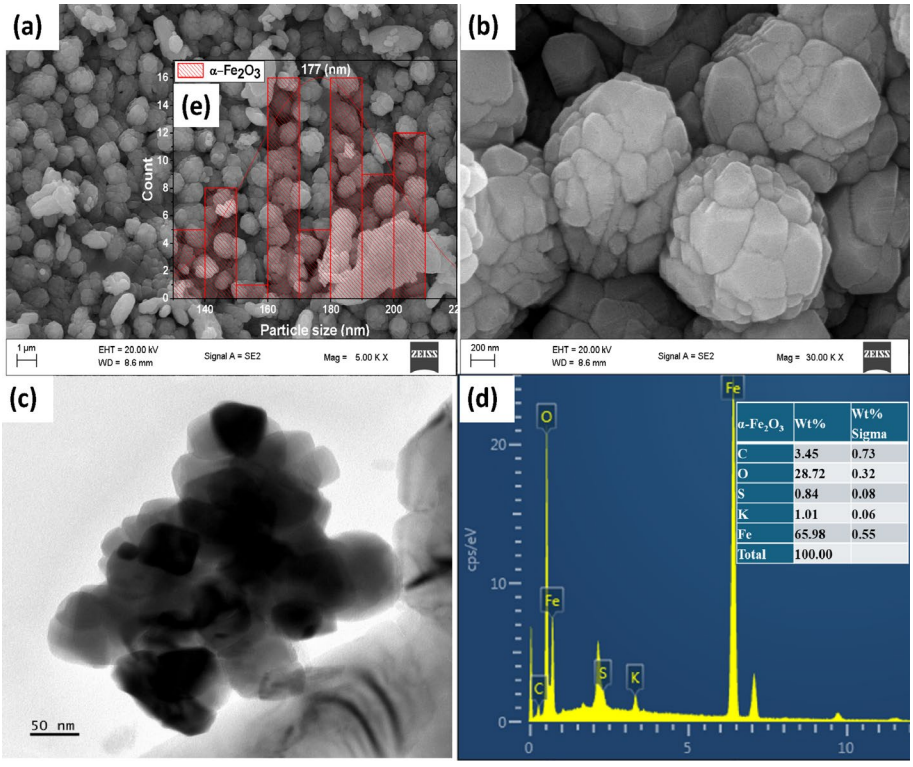


Fig. 6 SEM micrograph at **a** low, **b** high magnification, **c** TEM images, **d** EDX spectrum, and inset (e) particle size distribution histogram of α-Fe_2O_3 nanoparticles synthesized using aqueous extract of *Sorghum bicolor* leaf

presence of an excess of H^+ ions from the H_2O present on the surface of the nanoparticles [65]. However, the capping role of the phytocomponent obtained from the plant can protect the nanoparticles from agglomeration [66]. The particle size distribution histogram obtained from the SEM images shows that the agglomerated particles have an average size of 177 nm. This large size could be ascribed to fusion of the individual particles to form large spherical agglomerates. The TEM analysis (Fig. 6c) also showed highly agglomerated spherical morphology with no distinct edge. Green synthesized nanoparticles can give rise to varying sizes and morphologies such as squares, triangles, and spheres [67]. This variation has been attributed to the effect of the capping agent derived from compounds found in the leaf extracts and the synthesis temperature. Figure 6d presents the EDX spectrum of the α-Fe_2O_3 nanoparticles, which shows the elemental composition and confirms that iron (Fe) and oxygen (O) are the major components of the nanoparticles. The presence of potassium (K) and sulfur (S) could be from the plant extract, while the carbon (C) peak found could be ascribed to the emission from the carbon ribbon used during the analysis.

3.6 Anticancer evaluation of α-Fe_2O_3-NPs

Table 3 presents the cytotoxic effects of αFe_2O_3 nanoparticles and the standard chemotherapeutic agent, 5-fluorouracil (5-FU), on HeLa and HEK293 cell lines at different concentrations (10, 25, 50, and 100 µg/mL). The prepared α-Fe_2O_3-NPs demonstrated cytotoxic effects against HeLa and HEK293 cell lines, though their potency was lower than that of the standard chemotherapeutic agent 5-FU. The percentage viability of Hela and HEK 293 cell lines at different concentrations of 5-Fu and α-Fe_2O_3 is presented in

Table 3 HeLa and HEK293 cell line viability (%) at varying α-Fe_2O_3-NPs concentrations

Sample	10 μg/mL^{-1}	25 μg/mL^{-1}	50 μg/mL^{-1}	100 μg/mL^{-1}	IC_{50}
HeLa					
5-FU	78.24 ± 0.015	59.16 ± 0.048	52.21 ± 0.019	39.15 ± 0.031	17.46
α-Fe_2O_3	86.49 ± 0.119	58.06 ± 0.087	25.89 ± 0.029	13.03 ± 0.050	26.31
HEK293					
5-FU	77.19 ± 0.035	54.36 ± 0.014	39.87 ± 0.033	13.76 ± 0.025	6.71
α-Fe_2O_3	83.73 ± 0.071	74.74 ± 0.040	69.32 ± 0.017	39.00 ± 0.072	69.19

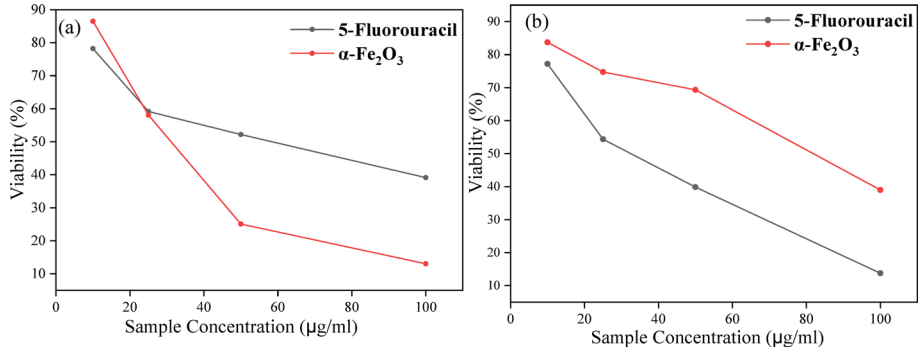


Fig. 7 Percentage viability of **a** HeLa cell line and **b** HEK293 cell line at different concentrations of 5-Fu and α-Fe_2O_3

Fig. 7. The viability of HeLa cells decreased in a dose-dependent manner upon exposure to α-Fe_2O_3-NPs, dropping from 86.49% at 10 μg/mL to 13.03% at 100 μg/mL, with an IC_{50} of 26.31 μg/mL. In comparison, 5-FU exhibited greater cytotoxicity, reducing HeLa cell viability from 78.24% at 10 μg/mL to 39.15% at 100 μg/mL, with a lower IC_{50} of 17.46 μg/mL. The higher IC_{50} of α-Fe_2O_3-NPs suggests that a greater concentration is required to achieve 50% inhibition, indicating lower potency compared to 5-FU. However, the ability of α-Fe_2O_3-NPs to reduce cancer cell viability highlights their potential as anticancer agents, possibly through mechanisms such as oxidative stress induction, apoptosis activation, and disruption of cellular iron homeostasis [68].

Interestingly, α-Fe_2O_3-NPs exhibited significantly lower toxicity toward HEK293 normal cells compared to 5-FU. While 5-FU drastically reduced HEK293 cell viability from 77.19% at 10 μg/mL to 13.76% at 100 μg/mL, with a very low IC_{50} of 6.71 μg/mL, α-Fe_2O_3-NPs displayed a more gradual cytotoxic effect, maintaining higher viability across all tested concentrations and yielding an IC_{50} of 69.19 μg/mL. This substantial difference suggests that α-Fe_2O_3-NPs exhibit selective toxicity, preferentially targeting cancer cells while sparing normal cells. The observed selectivity may be attributed to differences in nanoparticle uptake, metabolic activity, and oxidative stress handling between cancerous and non-cancerous cells. Cancer cells typically exhibit increased nanoparticle internalization due to altered endocytotic pathways, as well as heightened susceptibility to ROS-mediated damage due to their already elevated oxidative stress levels [69]. In contrast, normal cells possess more robust antioxidant defense mechanisms, which may account for their increased resistance to α-Fe_2O_3-NP-induced cytotoxicity [70].

The cytotoxic effects of α-Fe_2O_3-NPs in HeLa cells can be linked to several biological mechanisms, including ROS generation, apoptosis induction, and ferroptosis. The enhanced oxidative stress caused by α-Fe_2O_3-NPs likely disrupts mitochondrial function, leading to DNA damage and activation of apoptotic pathways [71, 72]. Additionally,

Table 4 Evaluation of the anticancer potential of α-Fe_2O_3 nanoparticles synthesized from *Sorghum bicolor* extract in comparison to other α-Fe_2O_3 nanoparticles documented in the literature

Nanoparticle	Concentration (µg/mL)	IC50 (µg/mL)	% Cell viability	Ref
FeO	100	–	87.02	[68]
TR-FeO	140	–	76.09	[68]
Fe_2O_3	100	40.42	46.11	[75]
Fe_2O_3@ CuO	100	21.13	35.42	[75]
FeO_2	100	–	50	[76]
α-Fe_2O_3	104.6	50	50	[69]
α-Fe_2O_3	100	26.31	13.03	This study
α-Fe_2O_3	100	85.19	39.00	This study

Table 5 Antioxidant activity (%) of α-Fe_2O_3-NPs

Samples	Conc. (ppm)						IC_{50}
	31.25	62.5	125	250	500	1000	
Ascorbic acid	4.73 ± 0.02	12.26 ± 0.06	35.95 ± 0.04	40.04 ± 0.01	52.21 ± 0.00	65.20 ± 0.02	3.48
α-Fe_2O_3-NPs	23.63 ± 0.01	47.99 ± 0.11	55.99 ± 0.06	62.91 ± 0.01	71.81 ± 0.01	71.14 ± 0.13	168.83

Values are presented as the mean inhibition percentage (%) ± deviation ($n = 3$), with ascorbic acid serving as the standard

α-Fe_2O_3-NPs may interfere with iron metabolism, triggering ferroptosis, a non-apoptotic form of programmed cell death characterized by lipid peroxidation and membrane damage [69]. The progressive decline in cell viability at increasing α-Fe_2O_3-NP concentrations supports this hypothesis, as cancer cells rely heavily on iron homeostasis for survival and proliferation. The involvement of apoptosis is further suggested by the potential modulation of pro-apoptotic and anti-apoptotic proteins, such as Bax and Bcl-2, which regulate mitochondrial membrane integrity and caspase activation [70].

The differential cytotoxic effects observed in HeLa and HEK293 cells highlight the potential of α-Fe_2O_3-NPs as selective anticancer agents. Compared to 5-FU, α-Fe_2O_3-NPs demonstrate a more favorable safety profile by causing significantly less damage to normal cells. This suggests that α-Fe_2O_3-NPs could serve as a nanomedicine-based alternative to conventional chemotherapy, potentially reducing systemic toxicity and adverse side effects such as myelosuppression and gastrointestinal disturbances [68]. Additionally, the selective cytotoxicity of α-Fe_2O_3-NPs presents an opportunity for their use in combination therapy, where they could enhance the efficacy of traditional chemotherapeutics while mitigating their toxic effects on healthy tissues [73]. Hence, the findings of this study support the growing interest in metal-based nanoparticles for cancer therapy, particularly due to their unique physicochemical properties that enable targeted interactions with cancer cells [74]. Table 4 presents the evaluation of the anticancer potential of α-Fe_2O_3-NPs synthesized from *Sorghum bicolor* extract in comparison to other iron oxides, composites, and α-Fe_2O_3-NPs reported in the literature.

The data are presented as mean cell viability (%) ± standard deviation ($n = 3$), with fluorouracil serving as the reference standard.

3.7 Antioxidant activity analysis of α-Fe_2O_3-NPs

Table 5; Fig. 8 present the antioxidant activity of α-Fe_2O_3-NPs against ascorbic acid at varying concentrations (31.25–1000 ppm). The inhibition percentage increased in a concentration-dependent manner for both α-Fe_2O_3-NPs and ascorbic acid. However, ascorbic acid demonstrated superior antioxidant efficacy. At doses of 31.25 and 62.5 ppm,

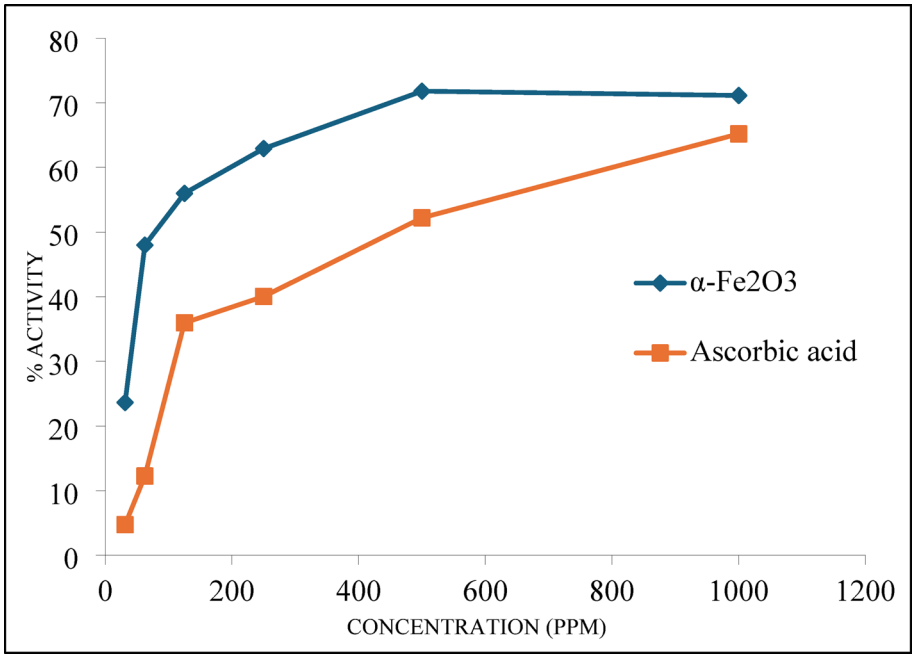


Fig. 8 Radical scavenging activity (%) of α-Fe_2O_3-NPs and ascorbic acid at various concentration

α-Fe_2O_3-NPs exhibited inhibition rates of 23.63% and 47.99%, respectively, while ascorbic acid showed 4.73% and 12.26% inhibition at the same concentrations. However, the IC_{50} value of α-Fe_2O_3-NPs (168.83 ppm) was much higher than ascorbic acid (3.48 ppm), indicating that a greater concentration α-Fe_2O_3-NPs was needed to achieve 50% radical inhibition. Despite the higher IC_{50}, the strong antioxidant activity observed in α-Fe_2O_3-NPs at higher concentrations suggests their potential role in combating oxidative stress, which is involved in various pathological conditions, such as cancer, inflammatory diseases, and neurodegenerative disorders.

The antioxidant capacity of α-Fe_2O_3-NPs can be attributed to several underlying mechanisms. One key pathway involves their ability to neutralize ROS and reactive nitrogen species (RNS) through electron donation, thereby preventing oxidative damage to vital biomolecules such as lipids, proteins, and DNA [77]. This redox activity is likely facilitated by the iron component of α-Fe_2O_3-NPs, which can participate in Fenton and Haber-Weiss reactions, influencing cellular oxidative balance. While this redox cycling can be beneficial in scavenging free radicals, its effects can vary depending on the biological microenvironment, potentially shifting between protective and pro-oxidant roles [78]. Additionally, α-Fe_2O_3-NPs may enhance endogenous antioxidant defense systems by upregulating key enzymes such as superoxide dismutase (SOD), catalase (CAT), and glutathione peroxidase (GPx) [79]. These enzymes play critical roles in mitigating oxidative stress and maintaining cellular homeostasis, which could contribute to the overall protective effects observed with α-Fe_2O_3-NPs.

Beyond their direct antioxidant effects, α-Fe_2O_3-NPs may have significant therapeutic implications. The ability to modulate oxidative stress suggests potential applications in adjunctive cancer therapy, where α-Fe_2O_3-NPs could help protect normal cells from chemotherapy-induced oxidative damage while still exerting selective cytotoxicity on cancer cells [80]. Similarly, α-Fe_2O_3-NPs could be valuable in managing neurodegenerative diseases such as Alzheimer's and Parkinson's, where oxidative stress is a key driver

Table 6 Evaluation of the antioxidant potential of α-Fe_2O_3 nanoparticles synthesized from *Sorghum bicolor* extract in comparison to other reported iron oxide nanoparticles

Material	Plant extract	IC_{50}	Ref
Fe_2O_3	*Pheonix dactylifera*	26.4 mg/g	[83]
Fe_2O_3	*Ficus carcia*	12.12 mg/mL	[84]
Fe_xO_y-NPs	*Pheonix dactylifera* L.	2.12 mg/mL	[85]
α-Fe_2O_3	Ginger extract	312.11 µg/mL	[86]
IO-NPS	*Laurus nobilis*	122.57 µg/mL	[87]
IO-NPS	*Sageretia thea*	33.85 µg/mL	[70]
α-Fe_2O_3	*Sorghum bicolor*	168.83 ppm	This study

of neuronal damage and disease progression [80]. Their capacity to reduce oxidative burden could also be beneficial in tissue regeneration and wound healing, where excessive oxidative stress impairs cellular repair mechanisms. Furthermore, their anti-inflammatory potential may contribute to reducing oxidative damage in chronic inflammatory conditions. Thus, the result of the present study indicates that α-Fe_2O_3-NPs possess strong antioxidant properties that could be leveraged for various biomedical applications [81, 82]. Their ability to scavenge free radicals, modulate redox balance, and enhance endogenous defense mechanisms position them as promising candidates for therapeutic interventions aimed at reducing oxidative stress-related damage. Table 6 presents the evaluation of the antioxidant potential of α-Fe_2O_3 nanoparticles prepared from *Sorghum bicolor* extract in comparison to other biosynthesized iron oxide nanoparticles documented in the literature. NPs, can exhibit both antioxidant and anticancer activities, but these effects often operate through distinct and sometimes opposing mechanisms. Interestingly, NPs with lower antioxidant activity may demonstrate higher anticancer efficacy due to their ability to induce oxidative stress selectively in cancer cells. The mechanism of α-Fe_2O_3 NPs, with antioxidant properties scavenge free radicals, thereby reducing cellular stress and preventing damage to DNA, proteins, and lipids.

4 Conclusion

In conclusion, the green synthesis of hematite nanoparticles (α-Fe_2O_3 NPs) using *Sorghum bicolo*r leaf extracts provides an environmentally friendly and cost-effective approach to nanoparticles synthesis. The synthesized NPs exhibited a crystalline rhombohedral hematite phase with spherical morphology and elemental composition confirming Fe and O as major components. The biological evaluations demonstrated selective cytotoxicity towards HeLa cancer cells while sparing normal HEK293 cells, supporting the role of iron homeostasis in cancer cell survival. Although the potency was lower than the standard chemotherapeutic agent 5-FU, the concentration-dependent reduction in cell viability suggests potential biomedical applications. Overall, this study highlights the promising use of *Sorghum bicolor*-mediated α-Fe_2O_3 NPs in nanomedicine, warranting further exploration of their therapeutic potential.

Author contributions

L.D.M.: Writing – original draft, Methodology, Formal analysis. M.C.O.: Writing – original draft, Formal analysis. D.M.N.M: Conceptualisation. D.C.O.: Conceptualization, Writing – review & editing, Supervision, Funding acquisition, Project administration.

Funding

Open access funding provided by North-West University. This study was funded by the North-West University, South Africa (1K02799).

Data availability

"Data is provided within the manuscript".

Declarations

Consent for publication
All authors are aware of this submission.

Competing interests
The authors declare no competing interests.

Ethical approval
Not applicable.

Clinical trial number
Not applicable.

Received: 8 February 2025 / Accepted: 5 June 2025
Published online: 15 July 2025

References

1. Daimari J, Deka AK. Anticancer, antimicrobial and antioxidant activity of CuO–ZnO bimetallic nanoparticles: green synthesised from *Eryngium foetidum* leaf extract. Sci Rep. 2024;14(1):19506.
2. Muthuvel A, et al. Synthesis of ceo 2-NPs by chemical and biological methods and their photocatalytic, antibacterial and in vitro antioxidant activity. Res Chem Intermed. 2020;46:2705–29.
3. Rani N, et al. Plant-mediated synthesis of nanoparticles and their applications: a review. Mater Res Bull. 2023;163:112233.
4. Slootweg JC. Sustainable chemistry: green, circular, and safe-by-design. One Earth. 2024;7(5):754–8.
5. Antunes Filho S, et al. Biosynthesis of nanoparticles using plant extracts and essential oils. Molecules. 2023;28. https://doi.org/10.3390/molecules28073060.
6. Osman AI, et al. Synthesis of green nanoparticles for energy, biomedical, environmental, agricultural, and food applications: a review. Environ Chem Lett. 2024;22(2):841–87.
7. Muthuvel A, et al. Green synthesis of cerium oxide nanoparticles using *Calotropis procera* flower extract and their photocatalytic degradation and antibacterial activity. Inorg Chem Commun. 2020;119:108086.
8. Ogwuegbu MC, et al. Green synthesis of CuO nanoparticles using *Ligustrum lucidum* extract, and the antioxidant and antifungal evaluation. Mater Res Express. 2024;11(5):055010.
9. Kumar A, et al. Integrating green nanotechnology with sustainable development goals: a pathway to sustainable innovation. Discover Sustain. 2024;5(1):364.
10. Kurul F, Doruk B, Topkaya SN. Principles of green chemistry: building a sustainable future. Discover Chem. 2025;2(1):68.
11. Yiblet Y, Sisay M. Metal oxide nanoparticles as a promising method to reduce biotic stress in plant cell wall: a review. Heliyon. 2024;10(19):e37939.
12. Sabouri Z, et al. Green synthesis of Ag-Se doped ZnO-Co_3O_4 fivenary nanocomposite using Poly anionic cellulose and evaluation of their anticancer and photocatalyst applications. Chem Methodologies. 2024;8(3):164–76.
13. Sabouri Z, et al. Plant-based synthesis of cerium oxide nanoparticles using Rheum Turkestanicum extract and evaluation of their cytotoxicity and photocatalytic properties. Mater Technol. 2022;37(8):555–68.
14. Sabouri Z, et al. Phytoextract-mediated synthesis of Ag-doped ZnO–MgO–CaO nanocomposite using *Ocimum basilicum* L. seeds extract as a highly efficient photocatalyst and evaluation of their biological effects. Ceram Int. 2023;49(12):20989–97.
15. Alameen AS, Undre SB, Undre PB. Synthesis, dispersion, functionalization, biological and antioxidant activity of metal oxide nanoparticles: review. Nano Struct Nano Objects. 2024;39:101298.
16. Zare M, et al. Emerging trends for ZnO nanoparticles and their applications in food packaging. ACS Food Sci Technol. 2022;2(5):763–81.
17. Mandal C, Sahu M et al. Application of metal and metal oxide nanoparticles as potential antibacterial agents. In: Singh SP, editors. Nanomaterials and nanocomposites for environmental remediation. Singapore: Springer; 2021. P. 121–140.
18. Tong W, et al. Highly sensitive magnetic particle imaging of vulnerable atherosclerotic plaque with active myeloperoxidase-targeted nanoparticles. Theranostics. 2021;11(2):506–21.
19. Sharma P, et al. Capping agent-induced variation of physicochemical and biological properties of α-Fe_2O_3 nanoparticles. Mater Chem Phys. 2021;258:123899.
20. Tabasi H, et al. pH-responsive and CD44-targeting by Fe_3O_4/MSNs-NH_2 nanocarriers for oxaliplatin loading and colon cancer treatment. Inorg Chem Commun. 2021;125:108430.
21. Sabouri Z, et al. Design and preparation of amino-functionalized core-shell magnetic nanoparticles for photocatalytic application and investigation of cytotoxicity effects. J Environ Health Sci Eng. 2023;21(1):93–105.
22. Tabasi H, et al. Synthesis and characterization of amine-functionalized Fe_3O_4/Mesoporous silica nanoparticles (MSNs) as potential nanocarriers in drug delivery systems. J Porous Mater. 2022;29(6):1817–28.
23. Mishra M, Chun D-M. α-Fe_3O_4 as a photocatalytic material: a review. Appl Catal A Gen. 2015;498:126–141.
24. Pourmadadi M, et al. Role of Iron oxide (Fe_2O_3) nanocomposites in advanced biomedical applications: a state-of-the-art review. Nanomaterials. 2022;12. https://doi.org/10.3390/nano12213873.
25. Kuldeep Chand V, Navdeep G. Green energy applications of hematite (α-Fe_2O_3), Magnetite (Fe_3O_4), and Maghemite (γ-Fe_2O_3) nanoparticles based hydroelectric cell. In: Xiao-Lan H, editors. Iron oxide nanoparticles. Rijeka: IntechOpen. 2022.
26. Bakari H, et al. Sorghum (*Sorghum bicolor* L. Moench) and its main parts (by-products) as promising sustainable sources of value-added ingredients. Waste Biomass Valoriz. 2023;14(4):1023–44.
27. Pontieri P, et al. Nutritional composition, fatty acid content, and mineral content of nine Sorghum (Sorghum bicolor) inbred varieties. Foods. 2024;13. https://doi.org/10.3390/foods13223634.
28. Edo GI, et al. Green biosynthesis of nanoparticles using plant extracts: mechanisms, advances, challenges, and applications. BioNanoScience. 2025;15(2):267.

29. Singh P, et al. Biological synthesis of nanoparticles from plants and microorganisms. Trends Biotechnol. 2016;34(7):588–99.
30. Mbenga Y, et al. Facile biosynthesis of CaO nanoparticles using extract of Tulbaghia violacea and evaluation of their antibacterial and cytotoxicity activity. Inorg Chem Commun. 2023;151:110581.
31. Ejikeme C, Ezeonu CS, Eboatu AN. Determination of physical and phytochemical constituents of some tropical timbers Indigenous to Nigerdelta area of Nigeria. Eur Sci J. 2014;10(18):247–70.
32. Dinga E, et al. Biosynthesis of ZnO nanoparticles using Melia azedarach seed extract: evaluation of the cytotoxic and antimicrobial potency. OpenNano. 2022;8:100068.
33. Ahmmad B, et al. Green synthesis of mesoporous hematite (α-Fe_2O_3) nanoparticles and their photocatalytic activity. Adv Powder Technol. 2013;24(1):160–7.
34. Adeyemi JA, et al. Phospholipids modifications in human hepatoma cell lines (HepG2) exposed to silver and iron oxide nanoparticles. Arch Toxicol. 2020;94:2625–36.
35. Zannou O, et al. Red sorghum (*Sorghum bicolor*) leaf sheaths as source stable pigments. Discover Food. 2025;5(1):4.
36. Hassan OHA. Phytochemical screening and antibacterial activities of *Sorghum bicolor* leaves derived from in vitro culture. GSC Biol Pharm Sci. 2020;10(1):065–72.
37. Cadenas E, Packer L. Handbook of antioxidants, vol 712. New York: Marcel Dekker. 2002.
38. Huang L, et al. Green synthesis of iron nanoparticles by various tea extracts: comparative study of the reactivity. Spectrochim Acta Part A Mol Biomol Spectrosc. 2014;130:295–301.
39. Njagi EC, et al. Biosynthesis of iron and silver nanoparticles at room temperature using aqueous sorghum Bran extracts. Langmuir. 2011;27(1):264–71.
40. Demirezen DA, et al. Green synthesis and characterization of iron oxide nanoparticles using *Ficus carica* (common fig) dried fruit extract. J Biosci Bioeng. 2019;127(2):241–5.
41. Kumar PR, et al. High capacity and low cost spinel Fe_3O_4 for the Na-ion battery negative electrode materials. Electrochim Acta. 2014;146:503–10.
42. Man Z, et al. Preparation of cellulose nanocrystals using an ionic liquid. J Polym Environ. 2011;19:726–31.
43. Tan XY, Abd Hamid SB, Lai CW. Preparation of high crystallinity cellulose nanocrystals (CNCs) by ionic liquid solvolysis. Biomass Bioenergy. 2015;81:584–91.
44. Faix O. Fourier transform infrared spectroscopy. In: Methods in lignin chemistry. Springer; 1992. P. 83–109.
45. Bledzki A, et al. The effects of acetylation on properties of flax fibre and its polypropylene composites. Express Polym Lett. 2008;2(6):413–22.
46. Kabir M, et al. Effects of chemical treatments on hemp fibre structure. Appl Surf Sci. 2013;276:13–23.
47. Ridzuan M, et al. Characterisation of natural cellulosic fibre from *Pennisetum purpureum* stem as potential reinforcement of polymer composites. Mater Des. 2016;89:839–47.
48. Yan Z, et al. Lignin relocation contributed to the alkaline pretreatment efficiency of sweet sorghum Bagasse. Fuel. 2015;158:152–8.
49. Zou P, et al. Characterization and bioactivity of polysaccharides obtained from pine cones of *Pinus koraiensis* by graded ethanol precipitation. Molecules. 2013;18(8):9933–48.
50. Ali HR, Nassar HN, El-Gendy NS. Green synthesis of α-Fe_2O_3 using Citrus reticulum peels extract and water decontamination from different organic pollutants. Energy Source Part A Recov Util Environ Eff. 2017;39(13):1425–34.
51. Miri A, Khatami M, Sarani M. Biosynthesis, magnetic and cytotoxic studies of hematite nanoparticles. J Inorg Organomet Polym Mater. 2020;30(3):767–74.
52. Kauffman KL, et al. FT-IR study of CO_2 adsorption in a dynamic copper(II) benzoate—Pyrazine host with CO_2–CO_2 interactions in the adsorbed state. J Phys Chem C. 2011;115(5):1857–66.
53. Ouellette RJ, Rawn JD. 17—ethers and epoxides. In: Ouellette RJ, Rawn JD, editors. Organic chemistry, 2nd ed. Academic Press; 2018. P. 507–536.
54. Hjiri M. Highly sensitive NO_2 gas sensor based on hematite nanoparticles synthesized by sol–gel technique. J Mater Sci Mater Electron. 2020;31(6):5025–31.
55. Bhuiyan MSH et al. Green synthesis of iron oxide nanoparticle using *Carica papaya* leaf extract: application for photocatalytic degradation of remazol yellow RR dye and antibacterial activity. Heliyon. 2020;6(8).
56. Anu K, Hemalatha J. Magnetic and electrical conductivity studies of zinc doped Cobalt ferrite nanofluids. J Mol Liq. 2019;284:445–53.
57. Santoshi TS, et al. Structural and magnetic properties of α-Fe_2O_3 with lithium ferrite prepared using co-precipitation method and annealed at different temperatures. Chem Phys Impact. 2024;9:100717.
58. Kirik NP, et al. Influence of temperature and duration of α-Fe_2O_3Calcination on reactivity in hydrogen oxidation. J Sib Fed Univ Chem. 2023;16:66–77.
59. Vinayagam R, et al. Structural characterization of green synthesized α-Fe_2O_3 nanoparticles using the leaf extract of *Spondias dulcis*. Surf Interfaces. 2020;20:100618.
60. Laouini S. Green synthesis of iron nanoparticules using leaf extract from *Phoenix dactylifera* L. J Fundam Appl Sci. 2019;11(2):978–93.
61. Abid MA, Kadhim DA. Novel comparison of iron oxide nanoparticle Preparation by mixing iron chloride with Henna leaf extract with and without applied pulsed laser ablation for methylene blue degradation. J Environ Chem Eng. 2020;8(5):104138.
62. Anit J, et al. A simple polyol one-shot synthesis of maghemite and hematite from inexpensive precursors. Inorg Chem Commun. 2023;151:110590.
63. Sheena P, et al. Effect of calcination temperature on the structural and optical properties of nickel oxide nanoparticles. Наносистемы: Физика Химия Математика. 2014;5(3):441–9.
64. Onwudiwe DC et al. NiO nanoparticles by thermal decomposition of complex and evaluation of the structural, morphological, and optical properties. J Mol Struct. 2024; 139084.
65. Kaur H, et al. Expanding horizon: green synthesis of TiO_2 nanoparticles using Carica papaya leaves for photocatalysis application. Mater Res Express. 2019;6(9):095034.
66. Kumar PSM, Francis AP, Devasena T. Biosynthesized and chemically synthesized Titania nanoparticles: comparative analysis of antibacterial activity. J Environ Nanotechnol. 2014;3(3):73–81.

67. Srinivasan M, et al. Green synthesis and characterization of titanium dioxide nanoparticles (TiO_2 NPs) using Sesbania grandiflora and evaluation of toxicity in zebrafish embryos. Process Biochem. 2019;80:197–202.
68. Shah SS, et al. Facile green synthesis of Iron oxide nanoparticles and their impact on cytotoxicity, antioxidative properties and bactericidal activity. Iran Biomed J. 2024;28(2–3):71.
69. Yoonus J, Resmi R, Beena B. Evaluation of antibacterial and anticancer activity of green synthesized iron oxide (α-Fe_2O_3) nanoparticles. Mater Today Proc. 2021;46:2969–74.
70. Israeel M, et al. Potential biological applications of environment friendly synthesized iron oxide nanoparticles using *Sageretia thea* root extract. Sci Rep. 2024;14(1):28310.
71. An X, et al. Oxidative cell death in cancer: mechanisms and therapeutic opportunities. Cell Death Dis. 2024;15(8):556.
72. Huang R, et al. Dual role of reactive oxygen species and their application in cancer therapy. J Cancer. 2021;12(18):5543.
73. Tian H, et al. Enhancing the therapeutic efficacy of nanoparticles for cancer treatment using versatile targeted strategies. J Hematol Oncol. 2022;15(1):132.
74. Gurunathan S, et al. Nanoparticle-mediated combination therapy: two-in-one approach for cancer. Int J Mol Sci. 2018;19(10):3264.
75. Mohamed AT, et al. Facile synthesis of Fe_2O_3, Fe_2O_3@ CuO and WO_3 nanoparticles: characterization, structure determination and evaluation of their biological activity. Sci Rep. 2024;14(1):6081.
76. Kgosiemang IKR, et al. Green synthesis of Iron oxide and Iron dioxide nanoparticles using *Euphorbia tirucalli*: characterization and antiproliferative evaluation against three breast cancer cell lines. J Exp Nanosci. 2023;18(1):2276276.
77. Kurutas EB. The importance of antioxidants which play the role in cellular response against oxidative/nitrosative stress: current state. Nutr J. 2015;15:1–22.
78. Ngo V, Duennwald ML. Nrf_2 and oxidative stress: A general overview of mechanisms and implications in human disease. Antioxidants. 2022;11(12):2345.
79. Gusti AM, et al. Antioxidants-related superoxide dismutase (SOD), catalase (CAT), glutathione peroxidase (GPX), glutathione-S-transferase (GST), and nitric oxide synthase (NOS) gene variants analysis in an obese population: a preliminary case-control study. Antioxidants. 2021;10(4):595.
80. Balakrishnan PVV, Gajski G, Chitra KC. The effects of iron oxide nanoparticles on antioxidant capacity and response to oxidative stress in Mozambique tilapia (Oreochromis mossambicus, Peters 1852). Arh Hig Rada Toksikol. 2024;75(2):125–36.
81. Prakash M, et al. Iron oxide nanoparticles for inflammatory bowel disease: recent advances in diagnosis and targeted drug therapy. Appl Surf Sci Adv. 2024;19:100540.
82. Ansari SR, Mahajan J, Teleki A. Iron oxide nanoparticles for treatment and diagnosis of chronic inflammatory diseases: a systematic review. Wiley Interdisciplinary Reviews: Nanomed Nanobiotechnol. 2024;16(3):e1963.
83. Abdullah JAA, et al. Green synthesis and characterization of iron oxide nanoparticles by *Pheonix dactylifera* leaf extract and evaluation of their antioxidant activity. Sustainable Chem Pharm. 2020;17:100280.
84. Üstün E, et al. Green synthesis of iron oxide nanoparticles by using *Ficus carica* leaf extract and its antioxidant activity. Biointerface Res Appl Chem. 2022;12(2):2108–16.
85. Abdullah JAA, et al. Green synthesis of FexOy nanoparticles with potential antioxidant properties. Nanomaterials. 2022;12(14):2449.
86. Hilo DH, Ismail AH, Al-Garawi ZS. Green synthesis of A-Fe_2O_3 from ginger extract enhanced the potential antioxidant activity against DPPH. Al-Mustansiriyah J Sci. 2022;33(4):64–71.
87. Yassin MT, et al. Green synthesis, characterization, and antifungal efficiency of biogenic iron oxide nanoparticles. Appl Sci. 2023;13(17):9942.

Publisher's note

Springer Nature remains neutral with regard to jurisdictional claims in published maps and institutional affiliations.